Small-Animal SPECT and SPECT/CT: Important Tools for Preclinical Investigation*

Benjamin L. Franc[1], Paul D. Acton[2], Carina Mari[1,3], and Bruce H. Hasegawa[†1]

[1]Department of Radiology, Center for Molecular and Functional Imaging, University of California, San Francisco, San Francisco, California; [2]Johnson & Johnson Pharmaceutical Research and Development, Spring House, Pennsylvania, and Department of Radiology, Thomas Jefferson University, Philadelphia, Pennsylvania; and [3]Department of Radiology, Department of Veteran's Affairs Medical Center, San Francisco, California

The need to study dynamic biologic processes in intact small-animal models of disease has stimulated the development of high-resolution nuclear imaging methods. These methods are capable of clarifying molecular interactions important in the onset and progression of disease, assessing the biologic relevance of drug candidates and potential imaging agents, and monitoring therapeutic effectiveness of pharmaceuticals serially within a single-model system. Single-photon–emitting radionuclides have many advantages in these applications, and SPECT can provide 3-dimensional spatial distributions of γ- (and x-) ray–emitting radionuclide imaging agents or therapeutics. Furthermore, combining SPECT with CT in a SPECT/CT system can assist in defining the anatomic context of biochemical processes and improve the quantitative accuracy of the SPECT data. Over the past decade, dedicated small-animal SPECT and SPECT/CT systems have been developed in academia and industry. Although significant progress in this arena has been realized through system development and biologic application, further innovation continues to address challenges in camera sensitivity, spatial resolution, and image reconstruction and quantification. The innumerable applications of small-animal SPECT and SPECT/CT in drug development, cardiology, neurology, and oncology are stimulating further investment in education, research, and development of these dedicated small-animal imaging modalities.

Key Words: small-animal imaging; SPECT; SPECT/CT

J Nucl Med 2008; 49:1651–1663
DOI: 10.2967/jnumed.108.055442

Rapidly evolving knowledge of molecular biology has stimulated exploration of novel therapies targeting specific points in molecular pathways associated with cardiac disease, neurologic disorders, cancer, and many other pathologic processes. However, identifying the role of a molecule in a disease process modeled in vitro does not necessarily translate to an understanding of its interactions with other molecular processes in vivo. On the other hand, few of all disease processes can be fully studied in human patients because of logistical and ethical concerns. Small-animal models represent a critical bridge between discoveries at the molecular level and implementation of clinically relevant diagnostics or therapeutics. Emphasis is ever increasing that these models accurately recapitulate both the disease itself and the environment in which the key molecular processes take place. For example, xenograft mouse models of cancer are simple to develop but are not considered particularly useful in understanding molecular interactions involved in carcinogenesis. More sophisticated approaches, such as transgenic models using oncogene activation or tumor suppressor inactivation, have evolved to the point at which cancers may be induced in a spatially and temporally defined manner using deletion of specified genetic sequences with Cre recombinase (*1,2*). Sophisticated infrastructures have been developed to manage data related to small-animal models of disease and provide greater access to various mouse models for all investigators, exemplified by the Mouse Models of Human Cancer Consortium sponsored by the National Institutes of Health (*3*) (information is available at http://mouse.ncifcrf.gov/).

For many years, studies of small-animal models relied on tissue sectioning and microscopy or, in the case of radionuclide-based assays, tissue γ-counting and autoradiography after euthanasia. These methods limited the ability of researchers to study a single animal serially over time and required the tedious assembling of histologic or autoradiographic sections. In essence, the assembly of multiple snapshots from different animals was assumed to accurately represent a continuous molecular process. These limitations are now being overcome through the use of molecular imaging to study dynamic biologic processes in small-animal models of disease. Single-photon–emitting radionu-

Received Jul. 10, 2007; revision accepted Jul. 22, 2008.
For correspondence or reprints contact: Benjamin L. Franc, Radiological Associates of Sacramento, 1500 Expo Parkway, Sacramento, CA 95815.
E-mail: francbl@radiological.com
[†]Deceased.
*NOTE: FOR CE CREDIT, YOU CAN ACCESS THIS ACTIVITY THROUGH THE SNM WEB SITE (http://www.snm.org/ce_online) THROUGH OCTOBER 2009.

Dr. Hasegawa indicated he received research support from GE Healthcare, Philips Medical Systems, Inc., Siemens Medical Solutions, Inc., Cytogen Corporation, Inc., and Radiation Monitoring Devices, Inc. No other potential conflict of interest relevant to this article was reported.

clides have many advantages in these applications, including a range of half-lives, relatively simple radiolabeling chemistry, low cost, and broad availability. Nuclear imaging follows these tracers at nanomolar and picomolar levels to explain molecular interactions important in the onset and progression of disease, to investigate the biologic relevance of drug candidates and potential imaging agents in streamlined development methodologies, and to monitor the therapeutic effectiveness of pharmaceuticals within a single-model system. Over the past decade, the growth in these nuclear imaging applications has motivated academic and industrial development of both SPECT and PET systems designed specifically for small-animal imaging, with both becoming widely available and affordable. PET is well suited for small-animal imaging, possessing a high detection sensitivity and spatial resolution typically in the range of 1–2 mm. Importantly, PET extends use of ^{18}F-FDG and other positron-labeled biologic tracers into the preclinical realm as a biomarker for pharmaceutical development and for metabolic studies in the biologic sciences.

SPECT also has several characteristics well suited for small-animal imaging. For instance, SPECT records γ-rays directly after radionuclide emission, thereby gaining a theoretic advantage in spatial resolution over PET, for which resolution is currently limited by fundamental processes of positron emission and annihilation. SPECT also has the unique capability of imaging multiple probes labeled with different isotopes, thereby allowing the simultaneous study of multiple molecular or cellular events (Fig. 1). SPECT uses many radiopharmaceuticals widely applied in clinical nuclear medicine and therefore can be obtained from central radiopharmacies. In many cases, if a desired radiopharmaceutical is not commercially available or in clinical use, a relatively simple laboratory setup is required to produce such tracers using single-photon radiochemistry. Finally, small-animal SPECT studies generally cost less than other small-animal imaging methods, such as small-animal PET or small-animal MRI.

In this article, we review the current status of small-animal SPECT/CT design, quantitative ability, detector configurations, and various camera performances in the context of a sampling of applications in drug development, cardiology, neurology, and oncology.

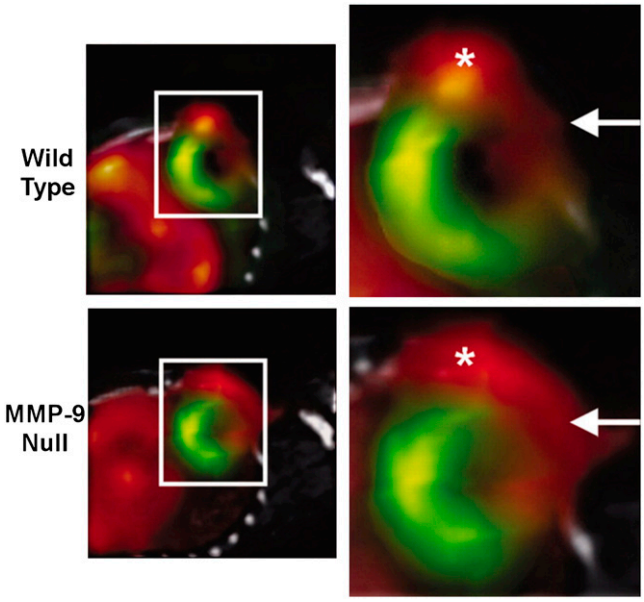

FIGURE 1. Coregistered in vivo micro-SPECT/CT images of ^{201}Tl to assess myocardial perfusion and ^{99m}Tc-NC100692 targeted at $\alpha_v\beta_3$ integrin to identify angiogenesis in wild-type and matrix metalloproteinase 9 (MMP-9) null mice. ^{99m}Tc-NC100692 micro-SPECT images (red) are fused with ^{201}Tl (green) and CT (gray) images to define uptake of $\alpha_v\beta_3$-targeted radiotracer relative to ^{201}Tl perfusion defect and anatomic structures within chest (CT performed with both ^{99m}Tc and ^{201}Tl data provides template for fusion). Boxed areas on left are magnified on right. Increased ^{99m}Tc-NC100692 uptake is seen in anterior-lateral infarct territory (arrows) and ^{99m}Tc-NC100692 activity associated with angiogenesis at thoracotomy site (*), demonstrating importance of simply knowing location of sternum as indicated on CT. ^{99m}Tc-NC100692 uptake also was noted in liver. (Reprinted with permission of (*117*).)

BACKGROUND

System Design

Although progress in the development and application of small-animal SPECT has been rapid to date, further innovation continues to address challenges in camera sensitivity, spatial resolution, and image reconstruction and quantification. The earliest small-animal SPECT systems were configured from a single scintillation camera operated with a collimator with a single pinhole aperture (Fig. 2A). These systems required scan times approaching 1 h, with levels of radioactivity (e.g., >37 MBq [>1 mCi] of ^{99m}Tc) that delivered relatively high levels of radiation dose to the animal. Small-animal SPECT still generally relies on pinhole collimation to achieve millimeter or submillimeter spatial resolution, but there is a trade-off between high resolution and lower sensitivity when using pinhole collimation secondary to the limited number of photons allowed through the pinhole to the face of the detector (Figs. 2C and 2D). The sensitivity of the single-pinhole system depends on the pinhole size but is typically only on the order of 1% or less for even large pinholes (e.g., 3 mm (*4*)). Systems with multiple detectors and effective use of the detector area with multipinhole collimators (Fig. 2B) have improved the trade-off between spatial resolution and detection sensitivity, increasing acquisition speed and enhancing volume localization for small foci of γ-emitting agents within the subject volume. However, the sensitivity of small-animal SPECT may never reach the sensitivity of small-animal PET (currently on the order of 1%–10% for commercial imaging systems).

Tomographic Reconstruction

In the clinic, SPECT traditionally has been performed by acquiring planar projection data with parallel-hole collimation at multiple angles around the object and then recon-

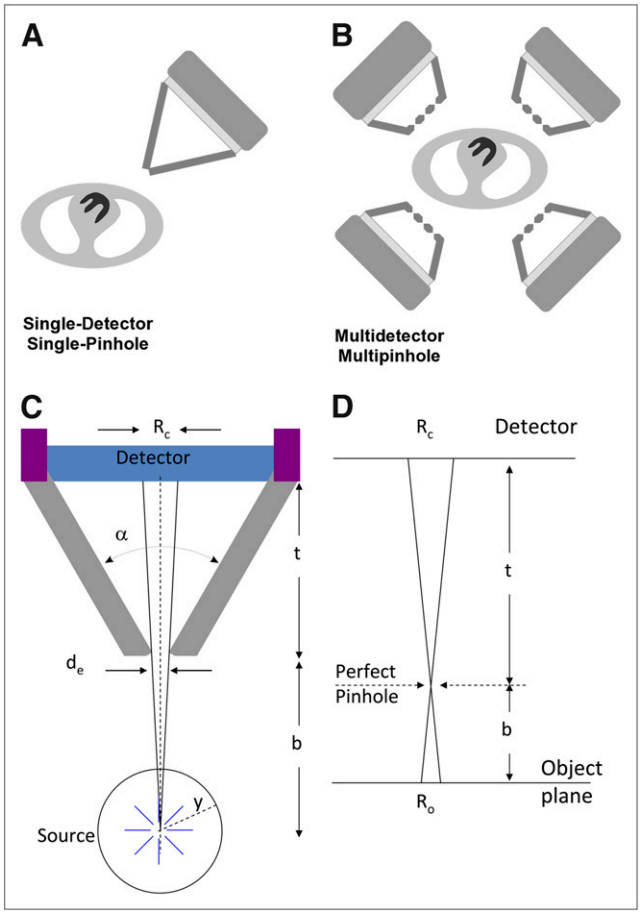

FIGURE 2. (A) Early small-animal SPECT systems were developed using single scintillation camera with single-pinhole collimator. (B) Modern small-animal SPECT systems use multiple detectors, each with multipinhole collimators. (C) Schematic of pinhole collimator geometry and relationships between object, its FOV, and its image on plane of detector. Angle between collimator walls (α), linear attenuation coefficient of collimator material (y), and pinhole diameter must be known to derive effective pinhole diameter (d_e). Geometric resolution measured on detector plane (R_c) is function of d_e, pinhole aperture-to-object distance (b), and pinhole aperture-to-detector distance (t). In figure, y equals radius of reconstruction circle and R_o equals detector point-spread function projected to object plane (spatial resolution in object plane at distance b from pinhole aperture). More detailed discussion of these relationships may be found in the references authored by Cherry et al., Metzler et al., and Metzler et al. (*118–120*). (D) Object is magnified by factor b/t onto plane of detector ($R_o = \left[\frac{b}{t}\right]R_c$); effective resolution can be improved by pinhole magnification.

structing 3-dimensional cross-sectional images using analytic techniques such as the well-known filtered backprojection (FBP) algorithm. However, small-animal SPECT typically relies on pinhole collimators that acquire projection data with cone-beam, rather than parallel-beam, geometry. Early small-animal SPECT systems used a tomographic reconstruction method known as the Feldkamp-Davis-Kress (FDK) algorithm (*5*), an analytic technique for reconstructing data acquired with cone-beam geometries, akin to reconstruction of parallel-beam data with FBP. However, because of the susceptibility of the FDK algorithm to propagation of noisy projection data and resulting streak artifacts and the degradation in spatial resolution resulting from a frequent need to apply a smoothing filter to decrease noise that passes the ramp filter in the algorithm, the FDK method has been generally replaced by iterative methods that model the physics of the acquisition process in the reconstruction algorithm.

A circular orbit with a pinhole collimator does not fully sample the object in the same way as is achieved with parallel-hole or fanbeam collimators. If uncorrected, the incomplete sampling can lead to incomplete projections, axial blurring, and image artifacts. Iterative reconstruction methods can account for the geometry of acquiring pinhole projection data, and more accurate sampling of the object can be obtained with alternative acquisition methods including those using multipinhole collimators, multiple detectors, and noncircular or helical orbits (*6*). Iterative reconstruction algorithms also can model the process of γ-ray penetration through the edges of the pinhole aperture (*6–8*) and thereby restore spatial resolution loss from septal penetration when using high-energy, photon-emitting radionuclides. Finally, iterative algorithms can compensate the radionuclide data for parallax errors and errors in positioning individual events when γ-rays strike the detector surface at oblique angles. Iterative reconstruction now is the dominant method of image reconstruction for both preclinical and clinical SPECT, because of its ability to recover or correct for some image-degrading effects and to generally offer images of higher visual quality and better quantitative accuracy than analytic reconstruction methods (*9,10*). Commercial small-animal SPECT systems typically claim up to submillimeter resolution using iterative reconstruction, but reconstructed resolutions based on FBP are more easily compared between systems.

SPECT/CT

SPECT can be combined with CT in an integrated small-animal imaging system (including some with PET as a third modality). The CT component of the SPECT/CT system is mounted in line with the SPECT, and both typically share a gantry. In most cases the CT consists of a microfocus x-ray tube source (tube current on the order of 1 mA at 50 kVp) and an x-ray detector (e.g., a charge-coupled device or a complementary metal oxide semiconductor with pixels on the order of 50 μm) with reconstructed resolutions below 100 μm. Alteration of tube voltages (e.g., range, 45–65 kVp) theoretically provides flexibility in contrast for soft tissues, and some success has been reported with contrast agents (*11*). Scanning may be helical or stepwise. CT reconstruction uses ray-tracing–based FBP.

SPECT/CT systems allow the radionuclide and CT data to be acquired and coregistered with minimal movement of the subject, often using a completely automated image registration method. CT provides excellent gross anatomic localization. The combination of SPECT with CT will likely be essential for the development of, and future use of, single-

photon–emitting probes. SPECT/CT will allow the anatomic localization and quantification of small amounts of increasingly specific radiolabeled probes taken up within the myocardium, small tumor metastases, neurologic system, or other anatomic structures in small-animal models of biology and disease. For example, new methods aiming for absolute quantification of molecular probes have coregistered a SPECT dataset with CT and have used a segmentation algorithm based on CT density levels to determine endocardial edges (*12*). Similar quantitative techniques also are being applied and developed for dosimetry and other applications in oncologic imaging and for in vivo pharmacokinetic assessment of new diagnostic and therapeutic agents.

In addition, just as in clinical applications, correlated structural data from CT images also can be used to derive a transmission map for object-specific attenuation correction. Typically, CT image values are converted to linear attenuation coefficient values using calibration curves obtained by imaging a CT calibration phantom containing multiple materials of known density. The attenuation map is then used to model the photon attenuation process in the forward and back projectors of an iterative SPECT reconstruction algorithm.

IMAGE QUANTIFICATION

Quantitative measurements always have presented challenges for SPECT but are vital for a multitude of small-animal imaging applications, such as measuring the dose-response curve for an experimental drug, monitoring tumor regression or recurrence after a novel treatment, or studying the changes in cerebral metabolism after a sensorimotor challenge. The requirements for accurate and quantitative data are complicated by limitations in the instrumentation and imaging process. γ-Rays emitted in tissue can be absorbed and scattered before entering the detector. The intrinsic resolution of the scanner can blur the radioactivity distribution and introduce error secondary to partial-volume effect, a phenomenon that arises in a target region whose dimensions are approximately equal to or smaller than the spatial resolution of the imaging system (*13*). Further, counting statistics can limit the temporal resolution of the detection system. For the measured activity to be a good approximation of the true distribution, many of these effects can be corrected (such as attenuation correction) or improved (such as resolution recovery in the reconstruction algorithm).

In human imaging, physical effects such as photon attenuation and scatter radiation can significantly perturb the quantitative accuracy of the SPECT data. However, whereas the small size of the animal presents a challenge to the instrumentation, it also has some benefits for quantitative measurements. Most notably, γ-rays traverse shorter tissue paths and thereby experience significantly less attenuation and scatter in mice and rats than in humans. This raises the fundamental question of whether scatter or attenuation correction is necessary in small-animal SPECT or whether these corrections are more apt to introduce unnecessary noise. Although only modest levels of attenuation are expected from small animals (usually rodents), this process still introduces a measurable error in relating the density of detected photons to the concentration of the radiopharmaceutical in an organ. The attenuation of detectable photons by soft tissue is estimated to be up to 50% when imaging ^{125}I and up to 25% when imaging ^{99m}Tc in rat-sized objects (*14*). Simulation studies suggest that for many isotopes, scatter may contribute approximately 20%–25% to the total counts in a rodent-sized object (*14,15*). However, in the case of ^{99m}Tc, less than 10% of all photons are probably scattered in rodent-sized objects. The effect of scatter is highly dependent on the geometry of both the source and the surrounding materials, but generally, compared with other sources of quantitative error in small-animal SPECT, scatter effect is not a substantial contributor to error. In addition, the overestimation errors typically resulting from scatter are offset by the relatively large underestimation errors caused by photon attenuation and partial-volume effects (*14*).

Correcting SPECT images for the effects of photon attenuation in tissue is relatively straightforward, either by using postprocessing of the images to extract an animal boundary or by, more accurately, using an external radiation source to map the attenuation distribution of the animal. Both processes can be performed by acquiring a CT scan of the animal immediately before or after the SPECT scan, with the animal in the same position during both SPECT and CT (*15*). Dual-modality SPECT/CT systems clearly simplify this process (*16,17*). The anatomic data from CT also could be used to correct the lower-resolution SPECT images for partial-volume effects, but, as is the case with radiographic imaging modalities in general, the poor soft-tissue contrast resolution of small-animal CT scanners may make this difficult in practice. Investigators also are developing methods to correct for scattered radiation.

Once the images are recorded as accurately as possible within the constraints of the equipment, extracting quantitative data that have physiologic relevance is a further complication. Tracer kinetic modeling provides the link between the distribution of radioactivity in tissue over time and the relevant physiologic parameters associated with a particular organ or disease state. This type of study generally requires rapid arterial blood sampling to provide the input function that drives the model. Obtaining arterial blood from small animals, such as mice (*18*) and rats (*19–21*), is challenging, particularly given their small total blood volume.

Simplified techniques for obtaining the arterial input function from the imaging data have been developed, such as measuring the blood-pool activity in the left ventricle at the same time as the organ of interest (*22–27*). Unfortunately, this has been limited to PET, because the axial field of view (FOV) of most pinhole SPECT systems is insufficient to include both the heart and another organ. Multipinhole systems may provide sufficient sensitivity and FOV to accommodate this technique, and a more recent small-

animal SPECT system, based on slit apertures rather than pinholes, may provide an opportunity for larger FOV imaging (*28*).

APPLICATION-BASED DESIGN REQUIREMENTS FOR SMALL-ANIMAL SPECT AND SPECT/CT

Drug Discovery and Evaluation

The preclinical validation of drug targeting, safety, and efficacy is strongly driving the use of small-animal SPECT in drug development. Drug-occupancy studies, often used in the evaluation of neurologic pharmaceuticals to understand the selectivity of drug binding in specific regions of the brain and the dependence of pre- and postsynaptic binding on endogenous levels of agonists (*29*), require repeated imaging of the binding of a drug to a receptor in a single animal in the presence of endogenous or exogenous ligands (*30*). The quantitative ability of SPECT in this application has been used in measuring ^{123}I-*N*-ω-fluoropropyl-2β-carbomethoxy-3β-(4-iodophenyl)-nortropane (^{123}I-FP-CIT) binding to dopamine transporters (DATs) in the rat brain after treatment with methylphenidate (*31*). SPECT also can help to validate the animal models themselves by evaluating the expression of various receptors or other targets of drug development in the animal's organ of interest.

In some cases, the temperospatial binding profiles of drugs can assist in predicting therapeutic outcome. Small-animal SPECT or SPECT/CT can assist in determining whether the biodistribution and pharmacokinetics of a radiolabeled form of a novel therapeutic drug (or novel imaging agent) are favorable for moving into clinical trials, and such methods have evaluated delivery via hematogenous, oral, and respiratory routes (*32–34*). Drugs also may be linked with moieties to guide their targeting or packaged in vehicles for more specific delivery. Small-animal SPECT has been used to identify the migration of ^{99m}Tc-labeled liposomes after intratumoral administration (*35*) and to study specific skeletal targeting of ^{125}I-labeled *N*-(2-hydroxypropyl)methacrylamide copolymer drug-delivery conjugates after intravenous administration (*36*). SPECT can be included in a multimodality small-animal imaging regimen to compare the location of the vehicle with the location of the drug in vivo. SPECT has been used in this manner to monitor macrophage carrier trafficking with colocalization of a fluorescently labeled nanoparticle loaded with antiretroviral therapy for HIV using ex vivo microscopy (*37*). As drug delivery becomes ever more targeted, the relationship between the biodistribution of the vehicle and the drug will remain important because the separation of the 2 in vivo can lead to failure of therapy in the clinic. Clearly, innovations in small-animal SPECT/CT technology will affect the speed of acquisition with ramifications for biodistribution and pharmacokinetic studies as well as image quantification. When kinetic models are necessary, current small-animal SPECT is limited in its temporal resolution, and small-animal PET remains a more applicable tool for such kinetic studies (*38*).

Because of its ability to measure the functional response of organs to a candidate therapy, small-animal SPECT can be used to understand the possible toxicities or secondary biochemical changes of a treatment or to explain observations seen in human clinical trials. For example, to investigate a potential connection between an administered therapy and aberrant blood pressures experienced by some patients in a recent phase I clinical trial of an experimental chemotherapy, SPECT/CT with ^{99m}Tc-annexin V was used to investigate whether the therapy was associated with cardiac apoptosis when administered to rat models (*39*).

The development and validation of imaging-based surrogate measurements, or biomarkers, for eventual use in clinical trials will likely be an area of growth for small-animal SPECT and SPECT/CT. In general, biomarkers have some biologic link to the process of the disease and changes in their levels may or may not parallel the severity or progression of the disease itself. By rendering a biomarker capable of being measured by a noninvasive means (e.g., radiolabeling it with a single-photon–emitting radionuclide for SPECT), it can be physically sampled less often. Small-animal SPECT can indirectly observe the therapeutic actions of pharmaceuticals (e.g., changes in receptor availability or changes in various surrogate markers) by imaging radiolabeled analogs of biomarkers and provide insight as to whether imaging can be used to monitor biomarkers of treatment failure or response in clinical trials (*40*). For example, ^{123}I-CIT SPECT of DAT function can act as a marker of the status of the nigrostriatal dopaminergic system during dopaminergic therapy for Parkinson disease (*41*). Small-animal SPECT can be helpful in understanding the dynamics of the target so that fluctuations in drug binding secondary to changes in expression of the binding site are not mistaken for resolution or progression of the disease itself, as may be seen in DAT imaging (*42*).

Other molecular indicators of mechanism or efficacy that have been measured in human and small-animal studies using SPECT include regional cerebral blood flow in the brain (*38,43,44*), temporal and spatial parameters of ^{111}In-labeled lymphocyte homing in inflammatory bowel disease (*45*), early neuronal ischemic injury levels evidenced by ^{99m}Tc-hydrazinonicotinic-annexin V in acute stroke (*46*), and uptake of ^{99m}Tc-hydrazinonicotinic-annexin V indicating apoptosis in malignancy (*47*). Objective, reproducible, and safe imaging–based biomarkers for SPECT will require substantial research. Clearly, the optimal situation is one in which a surrogate marker can be developed, standardized, and used in preclinical animal studies and can be carried through human trials. Small-animal SPECT promises to facilitate the translation of radiopharmaceuticals from mouse to human. The limiting factors in this development will be the relatively slow acquisition time of SPECT, which may be addressed using multipinhole systems. However, resulting improvements in acquisition time will need to be balanced with the potential to decrease levels of administered activity because repetitive use of radionuclide-based imaging bio-

markers could have potential ramifications on the biologic processes being studied.

Neurologic Applications

Imaging the brain in small animals with SPECT remains one of the most challenging applications of the modality because of the small size of brain structures, relatively low tracer uptake, and complex kinetics. However, it is also potentially one of the niche applications in small-animal imaging in which SPECT has significant advantages over other functional modalities, particularly PET (*13*). The main reasons for the advantage of SPECT, compared with PET, in brain imaging are the ability to push the spatial resolution to below 1 mm by fine-tuning the pinhole characteristics, the availability of longer-lived isotopes, and the high specific activity of most no-carrier-added SPECT tracers. Many PET tracers, particularly those labeled with ^{11}C, have a low specific activity, which may lead to significant occupancy of the target site by the tracer itself and possible pharmacologic effects.

Brain imaging demands the highest possible spatial resolution and sensitivity from equipment. In this application, it is an advantage that the brain is small, so the FOV can be limited to maximize resolution and sensitivity. Because uptake of most tracers in the brain is low (generally $<1\%$), and accurate quantification generally requires dynamic imaging with good temporal resolution, reasonable counting statistics may demand a high injected dose. Pinhole SPECT can provide accurate and quantitative imaging results from mouse (*48,49*) and rat (*50*) brain studies in the dopaminergic system (Fig. 3). Combining functional SPECT images with anatomic MRI data is particularly valuable in small-animal studies to delineate substructures within the brain (*51,52*).

Tracking uptake kinetics with brain imaging places further demands on the imaging equipment. Rapid dynamic scans are required to capture the true shape of the time–activity curve, coupled with high spatial resolution to provide adequate separation between the neighboring brain regions. These constraints have led to the development of multipinhole multiple-detector stationary SPECT systems (*53,54*); because the detectors do not need to rotate around the object, they can capture fast kinetics, which would otherwise be lost or blurred in a rotating scanner. Although the effect of radiation dose on small animals has not been studied in great detail, it is clear that brain-imaging studies may be one of the first applications in which multipinhole SPECT systems are a necessity because of the higher doses required for sufficient counting statistics in dynamic or quantitative SPECT. Indeed, simulation studies have been performed in which the multipinhole configuration is optimized specifically for mouse brain imaging (*55*), enabling the radiation dose to be reduced by an order of magnitude.

Cardiovascular Applications

Cardiovascular molecular imaging is an emerging and evolving field that integrates and motivates new imaging technology with the development of new cardiovascular

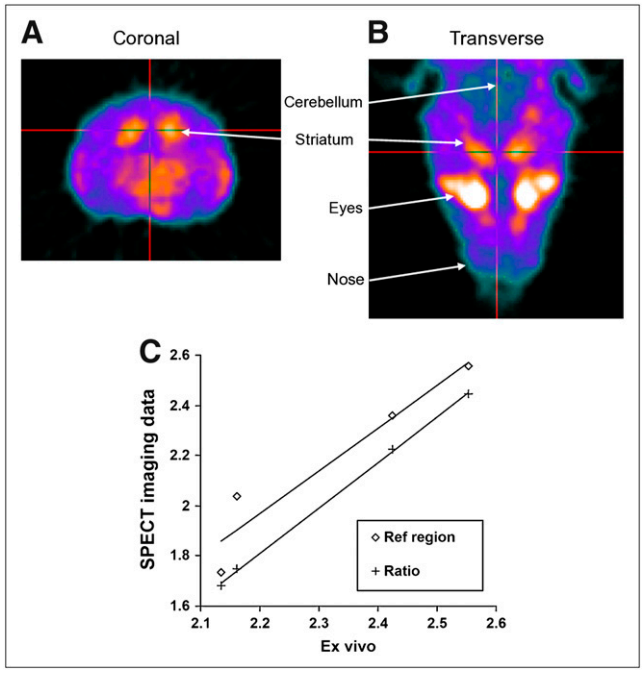

FIGURE 3. Coronal (A) and transverse (B) SPECT images showing uptake of DAT imaging agent ^{99m}Tc-[2-[[2-[[[3-(4-chlorophenyl)-8-methyl-8-azabicyclo[3,2,1]oct-2-yl]methyl](2-mercaptoethyl)amino]ethyl]amino]ethanethiolato(3-)-*N2,N2′,S2,S2′*]oxo-[1R-(exo-exo)] (TRODAT-1) in mouse brain 1 h after injection. Generally, greater localization of TRODAT-1 is seen in striatum than in cortical structures. (C) In vivo measurement of striatum-to-cerebellum ratio with SPECT, using kinetic modeling with extraction of input function from cerebellum (Ref region) and from relative striatum-to-cerebellum concentrations at equilibrium (Ratio), showed correlations of $R^2 = 0.92$ ($P = 0.04$) and $R^2 = 0.999$ ($P < 0.01$), vs. ex vivo measurements. (Reprinted with permission of (*48*).)

imaging agents (*56,57*). Imaging the heart of a mouse or a rat requires the spatial resolution of pinhole imaging because this organ and its vasculature are small. In addition, the rodent heart beats at a high rate (400–800 beats/min) and moves with every single breath; therefore, acquisition of images must often be performed with cardiac or respiratory gating. Several studies have used gated pinhole SPECT to obtain high-quality myocardial perfusion images in rats (*58,59*). A recent study achieved excellent quantitative accuracy with dedicated small-animal pinhole SPECT for in vivo measurement of small myocardial infarctions in rats (*60*). Processed gated SPECT can yield highly reproducible and accurate measurements of left ventricular volumes and ejection fraction in rats (*61*). Evaluation of myocardial wall motion abnormalities and myocardial thickening and quantification of myocardial flow reserve will be the next steps to be demanded from pinhole SPECT in small-animal myocardial perfusion studies.

Small-animal SPECT also can aid in the evaluation of new myocardial imaging agents in vivo. However, these tasks require the highest possible level of sensitivity and temporal resolution for dynamic studies, ideally with submillimeter spatial resolution. For example, a study in a rat animal model

of myocardial ischemia–reperfusion after left coronary artery occlusion with ^{99m}Tc-glucarate (a novel infarct-avid agent) used rapid sequence 3-dimensional imaging with a custom multidetector, multipinhole SPECT system (FASTSPECT; University of Arizona) to successfully quantify uptake and washout kinetics of the imaging agent with high resolution and fast dynamic acquisition (*62*). Targeting vascular endothelial growth factor receptors and $\alpha_v\beta_3$ (*63–66*) for imaging of ischemia-induced angiogenesis has the potential to complement routinely available clinical assessments of myocardial flow and to evaluate therapeutic angiogenic strategies. Apoptosis, or programmed cell death, occurs in many cardiovascular diseases and can be imaged in vivo with annexin V (*67*) labeled with ^{99m}Tc and other radionuclides. This approach has the potential for identifying an infarct, monitoring reperfusion therapy, or assessing heart transplant rejection (*68*). In vivo tracking of stem cells in cardiovascular disease is an exciting new area of research that requires, regardless of the stem cell origin, that the location and number of such cells be tracked, in vivo, over long periods (Fig. 4). Tracking small numbers of radiolabeled cells in the living body is extremely difficult, and an optimal solution does not yet exist (*69*).

One rapidly growing area of cardiovascular molecular imaging is the development of methods to characterize atherosclerotic plaques. All plaques do not carry the same risk of a later adverse myocardial event, and it would behoove physicians to target their interventions to only those plaques that showed biochemical or anatomic signs of potential rupture. Radiolabeled annexin V, Z2D3 (a smooth-muscle-cell antibody), and inhibitors to matrix metalloproteinases are SPECT agents that target specific pathophysiologic processes associated with atherosclerosis and have been used to characterize plaques in vivo (*64,70–72*). Anatomic localization and differentiation of plaque types remain challenges for small-animal CT and SPECT/CT because small-animal CT does not yet offer the acquisition speed or spatial resolution needed to image the small and motile coronary vessels of small animals. These represent areas in which profound advances both in imaging technology and in the development of new cardiovascular probes are needed to achieve the full potential of cardiovascular molecular imaging.

Oncologic Applications

γ-Ray photons from common radionuclides such as ^{99m}Tc easily penetrate the relatively thin soft tissues within the mouse, allowing the detection of molecules expressed around or on the surface of cancers within the animal. Thus, small-animal SPECT complements other molecular imaging modalities, such as optical techniques, particularly in transgenic models in which cancers can be deep within the imaging subject.

The recognition that gene expression is a dynamic phenomenon has increased the importance of characterizing various protein-mediated tumor processes serially in the laboratory. In this role, small-animal SPECT has been used to monitor cancer metastasis using cancer-specific targeting molecules (*73*); angiogenesis mediated by $\alpha_v\beta_3$ integrin expression with short-peptide radiopharmaceuticals during tumor growth, invasion, and metastasis (*74–77*); Her-2 expression using a Her-2 affibody (*78*); and prostate-specific membrane antigen (PSMA) expression levels in prostate cancer (Fig. 5) using small-molecule ligands for PSMA (*79*). Imaging small-animal models of cancer can illustrate the interaction of the tumor with its microenvironment, but further work is required to generate a sufficient library of imaging agents, because the translation of in vitro assays into SPECT agents is challenging (*74*). In the case of chemotherapy planning and evaluation for multidrug resistance, small-animal SPECT/CT has characterized several radiopharmaceuticals used to monitor the expression or activity of the transmembrane p-glycoprotein pump, including ^{99m}Tc tetrofosmin, ^{99m}Tc-sestamibi (*80*), and a Schiff base ^{67}Ga(III) complex (*81*), and compared their efflux with that of radiopharmaceuticals resistant to washout by p-glycoprotein–expressing tumors (*82*). These types of studies require rapid dynamic small-animal SPECT, similar to the need described earlier. The field of radiation oncology also has shown interest in using functional imaging to better define tumor volumes or characterize

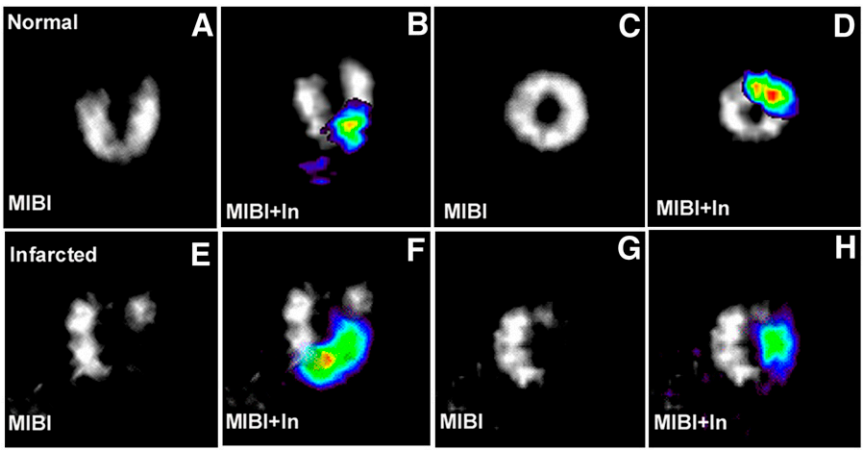

FIGURE 4. Cardiac long- and short-axis SPECT images of normal (A and C) and infarcted (E and G) heart using perfusion tracer ^{99m}Tc-sestamibi (MIBI). Signal from ^{111}In-labeled stem cells (In, color) was overlaid on gray-scale MIBI images for normal (B and D) and infarcted (F and H) heart.

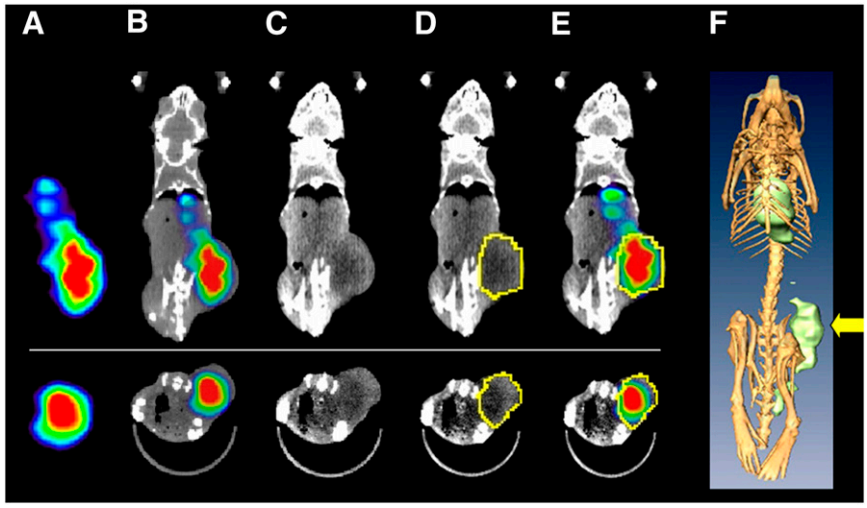

FIGURE 5. Small-animal SPECT/CT in oncology research. Coronal (A–E [top], F) and transaxial (A–E [bottom]) images from SPECT/CT study of LNCaP prostate cancer xenograft model 72 h after administration of antibody to PSMA labeled with ^{177}Lu. Tumor uptake is difficult to localize on SPECT images (A) but is easily localized anatomically on SPECT/CT overlay images (B). To quantify uptake of radiopharmaceutical, borders of tumor may be visualized on CT (C). Region of interest is selected on basis of CT (D) and applied to SPECT data (E). Three-dimensional renderings (F; arrow indicates tumor) may be helpful in better understanding anatomic relationships but rarely play role in quantification.

specific sites of poor tissue oxygenation in radiation treatment plans (*83*). Small-animal SPECT will play a role in the development of these techniques and in the definition and assessment of therapeutic response.

The ability to engineer tumor cells to express reporter genes, such as the herpes simplex virus type 1 thymidine kinase (HSV1-tk), has enabled noninvasive imaging of tumor cell volumes with a variety of modalities, including SPECT/CT. Once HSV1-tk phosphorylates the substrate 2-fluoro-2-deoxy-5-iodo-1-β-D-arbinofuranosyluracil (FIAU) labeled with ^{131}I or ^{123}I, the radiolabeled, monophosphorylated substrate is entrapped within the cell. The concentration of ^{131}I- or ^{123}I-FIAU within the tumor cells allows imaging of the location of the cells with SPECT (*84*). When imaged with small-animal SPECT, FIAU uptake has demonstrated a high correlation with the percentage of viable tumor cells and has been reliable in predicting response to therapy (*85*). When used to quantify protein expression after gene therapy, such as using ^{111}In-octreotide to monitor the expression of a somatostatin receptor gene therapy, quantitative small-animal SPECT/CT has demonstrated a strong correlation to in vitro γ-counting (*86*). In some cases, quantification has been improved in SPECT/CT by simply using the anatomic CT images to generate regions of interest instead of relying only on SPECT or planar scintigraphy (*87*). In addition to monitoring gene therapies, the effects of other therapies on gene transcription levels may also be measured using SPECT in the future. The use of radiolabeled antisense molecules for analysis of mRNA levels has been proposed (*88*), but the relatively small numbers of mRNA molecules to target for SPECT will be challenging, requiring high-sensitivity imaging systems.

Small-animal SPECT/CT will become increasingly important for the evaluation and advancement of molecular radiotherapeutics, as has been exemplified in the development of somatostatin receptor ligand analogs (*33*), development of folate-based radiopharmaceuticals (*89,90*), and enhancement of radiation dose delivery by adjuvant agents (*91*). As more molecular radiotherapeutics are realized and the quantitative accuracy of SPECT improves, some level of imaging-based dosimetry will likely become a requisite for Food and Drug Administration approval. Small-animal SPECT/CT can play a role in studies correlating dose and tumor eradication and dose to nontarget organs and unintended side effects.

ADVANCES IN SYSTEM DESIGN AND INSTRUMENTATION

Detector Technologies

The need for high spatial resolution and accurate quantification places technical demands on the performance of the radionuclide detector and the entire small-animal imaging system. Although early small-animal SPECT systems were implemented with clinical scintillation cameras, it is not surprising that imaging detectors have been developed and implemented specifically for small-animal SPECT. Newer dedicated systems for small-animal SPECT have implemented position-sensitive photomultiplier tubes and either segmented or continuous scintillation crystals and increased detector areas for greater magnification (*92–95*). Scintillation cameras with position-sensitive photomultiplier tubes require careful calibration to achieve good spatial uniformity and to correct their inherent pincushion distortion (similar to the calibration needed for block detector readout in PET). Nevertheless, this method has been implemented in several of the currently available small-animal SPECT systems now being marketed.

Some detectors developed for small-animal SPECT now alternatively incorporate semiconductor materials, such as cadmium zinc telluride (CZT) or silicon, as direct converters of γ-rays to electric signal. CZT is particularly attractive, as it can be segmented to offer intrinsic spatial resolution as high as approximately 380 μm (*16,96*). Furthermore, CZT can be operated at room temperature with excellent energy resolution, particularly important for imaging low-energy isotopes (e.g., ^{125}I). High-energy resolution also benefits algorithms

for rejecting scattered counts and simultaneous dual-isotope imaging for photopeaks that are close in energy (e.g., ^{99m}Tc and ^{123}I). CZT has not been used widely in clinical imaging as it is expensive and offers lower stopping power, yielding proportionally less detection efficiency in comparison with common scintillators such as thallium-doped sodium iodide. Furthermore, CZT can be prone to minute impurities associated with low-energy spectral tailing, pixel dropouts, hot spots, and nonuniform response (*97,98*).

Systems incorporating solid-state transducers, such as silicon avalanche photodiodes in place of photomultiplier tubes, have only recently reached performance levels sufficient for radionuclide imaging but offer a compact and rugged alternative to photomultiplier-based systems. Compact photodiode-based cameras have clinical applications in cardiac SPECT (*99*) and PET/MRI (*100,101*). Small-animal SPECT cameras are being designed (*102*) but have not yet appeared in commercially available systems.

Designs with Multiple Detectors and Multipinhole Collimators

The sensitivity of a SPECT system having a single detector operated with a single pinhole is relatively poor. For small-animal imaging, the poor sensitivity requires that compromises be made in the collimator design or imaging protocol to acquire adequate image statistics. One method of obtaining greater sensitivity is simply to inject the animal with additional radioactivity, but this approach may have significant ramifications for the biology being studied. As a first approximation of the levels of radiation to which small-animal tissues are subjected during SPECT studies, Funk et al. (*103*) used Monte Carlo modeling to derive S values (the S value, used in the MIRD schema (*104*), gives the absorbed dose per cumulated activity and per unit mass used) for mouse and rat bodies approximated as homogeneous ellipsoids, tabulated these S values for isotopes commonly used in small-animal imaging, and then used them to estimate the whole-body radiation dose to rodents using levels of radioactivity employed in published experiments and known radiopharmaceutical residence times. These calculations were performed using a central point source geometry to model a radiopharmaceutical with highly specific uptake within an organ or tumor and were then repeated using a homogeneously distributed source to model a radiopharmaceutical with nonspecific distribution. Estimates of whole-body doses in SPECT using examples of radiopharmaceutical doses from rodent studies in the literature ranged from less than 2 cGy (160 MBq of ^{99m}Tc in rats [200–250 g], assuming a biologic half-life of 1 h) to 90 cGy (740 MBq of ^{99m}Tc in 30-g mice, assuming a residence time of 3.2 h, a time similar to that of ^{99m}Tc-diethylenetriamine pentaacetic acid [DTPA] in humans). Whole-body doses to rats were found to be approximately a factor of 10 smaller than those calculated for mice for equivalent doses of radiopharmaceutical. As mice and rats often act only as hosts to xenograft or orthotopic tumor tissues, specific organ doses are often not even relevant; what matters is how the radiation affects the biology of interest (i.e., the effect on the tumor implant or other pathologic process). If anything, the concept of the whole-body dose underestimates the actual dose delivered to critical organs or tissues that are avid for a particular radiopharmaceutical. Many SPECT studies are longitudinal, providing multiple doses of a radiopharmaceutical to image multiple times over the course of a several-day or even a several-month experiment, and the cumulative dose to tissues is likely quite high. Effects on murine gene expression have been documented at doses of 20 cGy (*105*), and lethal doses on the order of several grays (e.g., doses causing mortality in 50% of mice over 30 d) have been reported to be approximately 7 Gy (*106,107*). Higher amounts of radioactivity also require larger volumes of injectate, which can lead to mechanical overload of the limited cardiovascular volume when dealing with mice (*108*).

Given an emphasis on maintaining high-resolution imaging with minimal effect on the biologic system studied, focus has been placed on increasing the detection efficiency of the SPECT system while maintaining or improving spatial resolution. Increasing the diameter of the pinhole improves sensitivity but at the cost of degrading spatial resolution (Fig. 2). Moving the pinhole closer to the subject increases sensitivity and improves resolution but proportionately reduces the FOV of the system. Consequently, researchers have shifted their attention to multiple detectors surrounding the subject or collimators with multiple pinholes to raise the geometric efficiency for detecting the emitted γ-rays. An important feature that distinguishes various designs of multipinhole collimators is whether the projections of the subject overlap, or multiplex, on the detector (Fig. 6). Multiplexing has consequences on the signal-to-noise ratio of the system and may make a system prone to artifacts. A nonoverlapping multipinhole system can use an existing clinical SPECT scanner, with absorbing septa placed between the pinholes to prevent cross-talk. This is the basis for the U-SPECT-I system (*53*), which uses a triple-head γ-camera and a custom-built cylindric collimator containing 75 gold pinholes and lead shielding positioned to prevent overlapping projections. The multipinhole design increases the system sensitivity roughly by a factor equal to the number of pinholes, which permits smaller-diameter pinholes (and, hence, better resolution) to be used while still obtaining reasonable counting statistics. Alternatively, by reducing the size of the individual SPECT detectors, it is possible to surround the subject by an array of such systems, each with a single-pinhole collimator. This is the basis for the FastSPECT II system (*54*), which uses 16 modular scintillation cameras to image the subject without any rotation. The main disadvantage of such a system is the increased cost to develop specialized detector modules.

Multiplexing systems that use a multipinhole collimator (up to 20 pinholes) and a single clinical scintillation camera, or systems that combine multipinhole collimators with scalable dedicated modular detectors and multipinhole

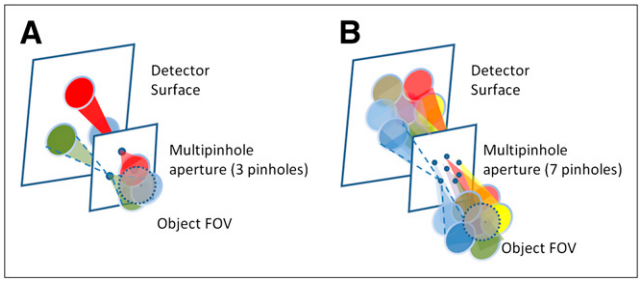

FIGURE 6. (A) Schematic of nonoverlapping multipinhole system. Object FOV is projected on detector surface through (in this case) 3 pinholes without overlap. Multipinhole design increases system sensitivity roughly by factor equal to number of pinholes. (B) Schematic of overlapping (multiplexed) multipinhole system. Object FOV is projected on detector surface through (in this case) 7 pinholes. In contrast to system in A, there is significant overlap of projections on detector surface in B.

collimators, have significant advantages, with increased sensitivity, expanded FOV, and improved object sampling. However, the increased counting rate obtained with overlapped multipinhole collimation does not necessarily yield the increased signal-to-noise ratio obtained with nonoverlapping projections, because of the ambiguity in the origin of each detected γ-ray (*109*). Although maximum-likelihood–based iterative reconstruction algorithms can provide a good estimate of the true activity distribution, there is a penalty imposed on the signal-to-noise ratio caused by the degree of overlap (*110*).

System Calibration

The high level of performance in small-animal SPECT, similar to SPECT systems used in the clinical setting, requires careful system calibration and quality control. Small-animal SPECT and SPECT/CT systems require precise mechanical alignment of both cameras and collimators with the system gantry. One calibration method for coding geometries has been discussed by Bequé et al. (*111*), who identified 7 parameters (e.g., detector angle, detector position, detector offset relative to the axis of rotation) required to accurately define the geometry of a detector rotating on a circular orbit. These authors concluded that all governing parameters could be measured from projection data acquired with 3 or more point sources within the FOV. A method to determine the remaining calibration parameters using a single point source, assuming that the detector tilt and the radius of rotation are known, has been discussed by Metzler et al. (*112*). Generally, these alignment measurements are acquired at the factory or by the service engineer to generate calibration parameters that then are recorded in a system file for subsequent calibration of the imaging system and reconstruction algorithm.

Once the system is in use, a quality-control program must monitor spatial resolution, spatial uniformity, energy resolution, and counting-rate response in a way similar to assessments performed for clinical SPECT systems. As it is common for many investigators and laboratories to share a single small-animal SPECT system, there is typically a need to frequently reconfigure the system (e.g., change collimators, alter the radius of rotation) for different tasks. The more frequently such changes are made, the more often will recalibration of the system be required. Whenever possible, an attempt should be made to dedicate the small-animal system to a single investigation. This becomes particularly important in longitudinal studies in which the reproducibility of data between time points can become difficult when there have been interval calibrations or simply mild misalignments secondary to the mechanical stress of multiple collimator changes.

The reliance on iterative reconstruction also introduces another level of calibration for the small-animal SPECT systems. As mentioned previously, iterative reconstruction algorithms can include a model of the imaging system, defined by parameters such as the pinhole–detector distance, the distance between the pinhole and the center of rotation, point-by-point nonuniformities in detector sensitivity (*113*), and septal penetration of the pinhole aperture (*114*). Traditionally, these factors are introduced by calculating the elements in the system matrix, which relates the counting rate recorded by each detector element to the radionuclide concentration at each point of the reconstruction volume (*115*). The system matrix then is incorporated into an iterative algorithm that reconstructs the radionuclide concentrations in the object from the ensemble of data recorded by each detector element at each projection angle. Improvements in spatial resolution translate to a larger system matrix. With recent advances in computational memory (and recent decreases in the cost of memory), even the large system matrices associated with high-resolution pinhole SPECT are typically stored and then retrieved for the iterative reconstruction. As a result, it is important to measure the system matrix carefully and at high precision (particularly when performing high-resolution pinhole SPECT) so that it is not perturbed by statistical uncertainties introduced by inadequate numbers of events. Further, given knowledge of the size and shape of the subject in the scanner from, for example, a CT or transmission scan, additional factors can be incorporated into the system matrix to account for scatter and attenuation of γ-rays. These additional factors generally are computed using Monte Carlo simulated data, which can account for inhomogeneous subjects (*116*).

CONCLUSION

Over the past decade, dedicated small-animal SPECT and SPECT/CT cameras have been developed in academia and industry. The rapid growth in interest in small-animal SPECT has been driven in large part by demand for streamlined drug development and the need for tools to translate understanding of fundamental molecular processes at the cellular level to clinically relevant therapeutics and interventions. Although significant progress in small-

animal SPECT and SPECT/CT has been realized through development and application, further innovation continues to address challenges in camera sensitivity, spatial resolution, and image reconstruction and quantification. Although imaging single-photon–emitting radionuclides with SPECT or SPECT/CT offers several advantages in study flexibility and radiochemistry complexity and costs, small-animal PET is currently the most sensitive and quantitatively accurate nuclear imaging modality. Many of the current shortcomings of small-animal SPECT and SPECT/CT are beginning to be overcome by newer generation SPECT/CT cameras and reconstruction algorithms. The innumerable applications of small-animal SPECT and SPECT/CT in drug development, cardiology, neurology, and oncology necessitate further investment in their research and development and education in guiding their applications. New modalities, such as SPECT/MRI, could offer the advantage of additional anatomic and functional information, generating the next level of multimodality molecular imaging.

ACKNOWLEDGMENTS

We gratefully acknowledge support from the National Institutes of Health grants 5 R01 NS048315, 1 R01 E001809, 1 R01 EB, 5 R01 EB000348, 5 R44 CA095936, and 1 R21 EB006373 and the University of California, San Francisco, Department of Radiology, seed grant 06-03. In addition, we dedicate this work to our colleague Bruce Hasegawa, who has been a valued friend, teacher, and mentor and an inspiration to so many of us over the years.

REFERENCES

1. Marusyk A, Degregori J. Building a better model of cancer. *Cell Div.* 2006;1:24.
2. Carver BS, Pandolfi PP. Mouse modeling in oncologic preclinical and translational research. *Clin Cancer Res.* 2006;12:5305–5311.
3. Peters LL, Robledo RF, Bult CJ, Churchill GA, Paigen BJ, Svenson KL. The mouse as a model for human biology: a resource guide for complex trait analysis. *Nat Rev Genet.* 2007;8:58–69.
4. Figueroa SD, Winkelmann CT, Volkert WA, Hoffman TJ. Performance characteristics of an integrated small animal SPECT/CT unit. In: Yu B, ed. *2005 IEEE Nuclear Science Symposium Conference Record.* Vol. 3. Piscataway, NJ: IEEE; 2005:1752–1756.
5. Feldkamp LA, Davis LC, Kress JW. Practical cone-beam algorithm. *J Opt Soc Am.* 1984;A1:612–619.
6. Smith MF, Jaszczak RJ. An analytic model of pinhole aperture penetration for 3D pinhole SPECT image reconstruction. *Phys Med Biol.* 1998;43:761–775.
7. Deloar HM, Watabe H, Aoi T, Iida H. Evaluation of penetration and scattering components in conventional pinhole SPECT: phantom imaging using Monte Carlo simulation. *Phys Med Biol.* 2003;48:995–1008.
8. Smith MF, Jaszczak RJ. The effect of gamma ray penetration on angle-dependent sensitivity for pinhole collimation in nuclear medicine. *Med Phys.* 1997;24:1701–1709.
9. Bruyant PP. Analytic and iterative reconstruction algorithms in SPECT. *J Nucl Med.* 2002;43:1343–1358.
10. Israel-Jost V, Choquet P, Salmon S, Blondet C, Sonnendrucker E, Constantinesco A. Pinhole SPECT imaging: compact projection/backprojection operator for efficient algebraic reconstruction. *IEEE Trans Med Imaging.* 2006;25:158–167.
11. Tsui BM, Mok G, Wang Y, et al. High-resolution small animal SPECT/CT imaging of atherosclerotic plaques in ApoE−/− mice using Tc-99m annexin-V and contrast enhanced CT [abstract]. *J Nucl Med.* 2007;48(suppl 2):103P.
12. Li S, Dobrucki LW, Sinusas AJ, Liu YH. A new method for SPECT quantification of targeted radiotracers uptake in the myocardium. *Med Image Comput Comput Assist Interv Int Conf Med Image Comput Comput Assist Interv.* 2005;8(pt 2):684–691.
13. Acton PD, Kung HF. Small animal imaging with high resolution single photon emission tomography. *Nucl Med Biol.* 2003;30:889–895.
14. Hwang AB, Franc BL, Gullberg GT, Hasegawa BH. Assessment of the sources of error affecting the quantitative accuracy of SPECT imaging in small animals. *Phys Med Biol.* 2008;53:2233–2252.
15. Hwang AB, Hasegawa BH. Attenuation correction for small animal SPECT imaging using x-ray CT data. *Med Phys.* 2005;32:2799–2804.
16. Kastis GA, Furenlid LR, Wilson DW, Peterson TE, Barber HB, Barrett HH. Compact CT/SPECT small-animal imaging system. *IEEE Trans Nucl Sci.* 2004;51:63–67.
17. Weisenberger AG, Wojcik R, Baradley EL, et al. SPECT-CT system for small animal imaging. *IEEE Trans Nucl Sci.* 2003;50:74–79.
18. Toyama H, Ichise M, Liow JS, et al. Absolute quantification of regional cerebral glucose utilization in mice by ^{18}F-FDG small animal PET scanning and 2-^{14}C-DG autoradiography. *J Nucl Med.* 2004;45:1398–1405.
19. Fujita M, Zoghbi SS, Crescenzo MS, et al. Quantification of brain phosphodiesterase 4 in rat with (*R*)-[^{11}C]Rolipram-PET. *Neuroimage.* 2005;26:1201–1210.
20. Meyer PT, Circiumaru V, Cardi CA, Thomas DH, Bal H, Acton PD. Simplified quantification of small animal [^{18}F]FDG PET studies using a standard arterial input function. *Eur J Nucl Med Mol Imaging.* 2006;33:948–954.
21. Shimoji K, Ravasi L, Schmidt K, et al. Measurement of cerebral glucose metabolic rates in the anesthetized rat by dynamic scanning with ^{18}F-FDG, the ATLAS small animal PET scanner, and arterial blood sampling. *J Nucl Med.* 2004;45:665–672.
22. Green LA, Gambhir SS, Srinivasan A, et al. Noninvasive methods for quantitating blood time-activity curves from mouse PET images obtained with fluorine-18-fluorodeoxyglucose. *J Nucl Med.* 1998;39:729–734.
23. Green LA, Nguyen K, Berenji B, et al. A tracer kinetic model for ^{18}F-FHBG for quantitating herpes simplex virus type 1 thymidine kinase reporter gene expression in living animals using PET. *J Nucl Med.* 2004;45:1560–1570.
24. Huang Y, Narendran R, Bae SA, et al. A PET imaging agent with fast kinetics: synthesis and in vivo evaluation of the serotonin transporter ligand [^{11}C]2-[2-dimethylaminomethylphenylthio)]-5-fluorophenylamine ([^{11}C]AFA). *Nucl Med Biol.* 2004;31:727–738.
25. Kim J, Herrero P, Sharp T, et al. Minimally invasive method of determining blood input function from PET images in rodents. *J Nucl Med.* 2006;47:330–336.
26. Yee SH, Jerabek PA, Fox PT. Non-invasive quantification of cerebral blood flow for rats by microPET imaging of ^{15}O labelled water: the application of a cardiac time-activity curve for the tracer arterial input function. *Nucl Med Commun.* 2005;26:903–911.
27. Yee SH, Lee K, Jerabek PA, Fox PT. Quantitative measurement of oxygen metabolic rate in the rat brain using microPET imaging of briefly inhaled ^{15}O-labelled oxygen gas. *Nucl Med Commun.* 2006;27:573–581.
28. Walrand S, Jamar F, de Jong M, Pauwels S. Evaluation of novel whole-body high-resolution rodent SPECT (Linoview) based on direct acquisition of linogram projections. *J Nucl Med.* 2005;46:1872–1880.
29. Nikolaus S, Larisch R, Wirrwar A, et al. [^{123}I]Iodobenzamide binding to the rat dopamine D_2 receptor in competition with haloperidol and endogenous dopamine: an in vivo imaging study with a dedicated small animal SPECT. *Eur J Nucl Med Mol Imaging.* 2005;32:1305–1310.
30. Maziere B, Loc'h C. Use of bromine-76 and iodine-123 radiohalogenated tracers in the drug development process. *Curr Pharm Des.* 2001;7:1931–1943.
31. Nikolaus S, Wirrwar A, Antke C, et al. Quantitation of dopamine transporter blockade by methylphenidate: first in vivo investigation using [^{123}I]FP-CIT and a dedicated small animal SPECT. *Eur J Nucl Med Mol Imaging.* 2005;32:308–313.
32. Dolovich M, Labiris R. Imaging drug delivery and drug responses in the lung. *Proc Am Thorac Soc.* 2004;1:329–337.
33. Ginj M, Chen J, Walter MA, Eltschinger V, Reubi JC, Maecke HR. Preclinical evaluation of new and highly potent analogues of octreotide for predictive imaging and targeted radiotherapy. *Clin Cancer Res.* 2005;11:1136–1145.
34. Hirata M, Mori T, Soga S, Umeda T, Ohmomo Y. In vivo evaluation of radioiodinated 1-[2-(3,4-dimethoxyphenyl)ethyl]-4-(3-phenylpropyl)-piperazine derivatives as new ligands for sigma receptor imaging using single photon emission computed tomography. *Biol Pharm Bull.* 2006;29:2009–2015.
35. Bao A, Phillips WT, Goins B, et al. Potential use of drug carried-liposomes for cancer therapy via direct intratumoral injection. *Int J Pharm.* 2006;316:162–169.
36. Wang D, Sima M, Mosley RL, et al. Pharmacokinetic and biodistribution studies of a bone-targeting drug delivery system based on *N*-(2-hydroxypropyl)-methacrylamide copolymers. *Mol Pharm.* 2006;3:717–725.
37. Dou H, Destache CJ, Morehead JR, et al. Development of a macrophage-based nanoparticle platform for antiretroviral drug delivery. *Blood.* 2006;108:2827–2835.

38. Brooks DJ. Positron emission tomography and single-photon emission computed tomography in central nervous system drug development. *NeuroRx.* 2005;2:226–236.
39. Schimmel K, Bennink R, de Bruin K, et al. Absence of cardiotoxicity of the experimental cytotoxic drug cyclopentenyl cytosine (CPEC) in rats. *Arch Toxicol.* 2005;79:268–276.
40. Holtke C, Law MP, Wagner S, et al. Synthesis, in vitro pharmacology and biodistribution studies of new PD 156707-derived ET_A receptor radioligands. *Bioorg Med Chem.* 2006;14:1910–1917.
41. Brooks DJ, Frey KA, Marek KL, et al. Assessment of neuroimaging techniques as biomarkers of the progression of Parkinson's disease. *Exp Neurol.* 2003; 184(suppl 1):S68–S79.
42. Winogrodzka A, Booij J, Wolters E. Disease-related and drug-induced changes in dopamine transporter expression might undermine the reliability of imaging studies of disease progression in Parkinson's disease. *Parkinsonism Relat Disord.* 2005;11:475–484.
43. Devous MD Sr. Single-photon emission computed tomography in neurotherapeutics. *NeuroRx.* 2005;2:237–249.
44. Trollor JN, Sachdev PS, Haindl W, Brodaty H, Wen W, Walker BM. Combined cerebral blood flow effects of a cholinergic agonist (milameline) and a verbal recognition task in early Alzheimer's disease. *Psychiatry Clin Neurosci.* 2006;60:616–625.
45. van Montfrans C, Bennink RJ, de Bruin K, et al. In vivo evaluation of ^{111}In-labeled T-lymphocyte homing in experimental colitis. *J Nucl Med.* 2004;45: 1759–1765.
46. Blankenberg FG, Kalinyak J, Liu L, et al. ^{99m}Tc-HYNIC-annexin V SPECT imaging of acute stroke and its response to neuroprotective therapy with anti-Fas ligand antibody. *Eur J Nucl Med Mol Imaging.* 2006;33:566–574.
47. Mandl SJ, Mari C, Edinger M, et al. Multi-modality imaging identifies key times for annexin V imaging as an early predictor of therapeutic outcome. *Mol Imaging.* 2004;3:1–8.
48. Acton PD, Choi SR, Plossl K, Kung HF. Quantification of dopamine transporters in the mouse brain using ultra-high resolution single-photon emission tomography. *Eur J Nucl Med.* 2002;29:691–698.
49. Acton PD, Hou C, Kung MP, Plossl K, Keeney CL, Kung HF. Occupancy of dopamine D_2 receptors in the mouse brain measured using ultra-high-resolution single-photon emission tomography and ^{123}IBF. *Eur J Nucl Med Mol Imaging.* 2002;29:1507–1515.
50. Booij J, de Bruin K, Habraken JB, Voorn P. Imaging of dopamine transporters in rats using high-resolution pinhole single-photon emission tomography. *Eur J Nucl Med Mol Imaging.* 2002;29:1221–1224.
51. Booij J, de Bruin K, de Win MM, Lavini C, den Heeten GJ, Habraken JB. Imaging of striatal dopamine transporters in rat brain with single pinhole SPECT and co-aligned MRI is highly reproducible. *Nucl Med Biol.* 2003;30: 643–649.
52. Scherfler C, Decristoforo C. Small animal imaging using a conventional gamma camera exemplified in studies on the striatal dopaminergic system. *Nucl Med Rev Cent East Eur.* 2006;9:6–11.
53. Beekman FJ, van der Have F, Vastenhouw B, et al. U-SPECT-I: a novel system for submillimeter-resolution tomography with radiolabeled molecules in mice. *J Nucl Med.* 2005;46:1194–1200.
54. Furenlid LR, Wilson DW, Chen YC, et al. FastSPECT II: a second-generation high-resolution dynamic SPECT imager. *IEEE Trans Nucl Sci.* 2004;51:631–635.
55. Cao Z, Bal G, Accorsi R, Acton PD. Optimization of multipinhole arrangements for quantitative mouse brain SPECT by Monte Carlo simulation. *2004 IEEE Nucl Sci Symp Conf Rec.* 2004;4:2470–2474.
56. Dobrucki LW, Sinusas AJ. Cardiovascular molecular imaging. *Semin Nucl Med.* 2005;35:73–81.
57. Tsui BM, Wang Y. High-resolution molecular imaging techniques for cardiovascular research. *J Nucl Cardiol.* 2005;12:261–267.
58. Hirai T, Nohara R, Hosokawa R, et al. Evaluation of myocardial infarct size in rat heart by pinhole SPECT. *J Nucl Cardiol.* 2000;7:107–111.
59. Yukihiro M, Inoue T, Iwasaki T, Tomiyoshi K, Erlandsson K, Endo K. Myocardial infarction in rats: high-resolution single-photon emission tomographic imaging with a pinhole collimator. *Eur J Nucl Med.* 1996;23:896–900.
60. Acton PD, Thomas D, Zhou R. Quantitative imaging of myocardial infarct in rats with high resolution pinhole SPECT. *Int J Cardiovasc Imaging.* 2006;22:429–434.
61. Vanhove C, Lahoutte T, Defrise M, Bossuyt A, Franken PR. Reproducibility of left ventricular volume and ejection fraction measurements in rat using pinhole gated SPECT. *Eur J Nucl Med Mol Imaging.* 2005;32:211–220.
62. Liu Z, Barrett HH, Stevenson GD, et al. High-resolution imaging with ^{99m}Tc-glucarate for assessing myocardial injury in rat heart models exposed to different durations of ischemia with reperfusion. *J Nucl Med.* 2004;45:1251–1259.
63. Blankenberg FG, Mandl S, Cao YA, et al. Tumor imaging using a standardized radiolabeled adapter protein docked to vascular endothelial growth factor. *J Nucl Med.* 2004;45:1373–1380.
64. Hua J, Dobrucki LW, Sadeghi MM, et al. Noninvasive imaging of angiogenesis with a ^{99m}Tc-labeled peptide targeted at $\alpha_v\beta_3$ integrin after murine hindlimb ischemia. *Circulation.* 2005;111:3255–3260.
65. Lu E, Wagner WR, Schellenberger U, et al. Targeted in vivo labeling of receptors for vascular endothelial growth factor: approach to identification of ischemic tissue. *Circulation.* 2003;108:97–103.
66. Meoli DF, Sadeghi MM, Krassilnikova S, et al. Noninvasive imaging of myocardial angiogenesis following experimental myocardial infarction. *J Clin Invest.* 2004;113:1684–1691.
67. Strauss HW, Narula J, Blankenberg FG. Radioimaging to identify myocardial cell death and probably injury. *Lancet.* 2000;356:180–181.
68. Blankenberg FG, Katsikis PD, Tait JF, et al. In vivo detection and imaging of phosphatidylserine expression during programmed cell death. *Proc Natl Acad Sci USA.* 1998;95:6349–6354.
69. Frangioni JV, Hajjar RJ. In vivo tracking of stem cells for clinical trials in cardiovascular disease. *Circulation.* 2004;110:3378–3383.
70. Khaw BA, Tekabe Y, Johnson LL. Imaging experimental atherosclerotic lesions in ApoE knockout mice: enhanced targeting with Z2D3-anti-DTPA bispecific antibody and ^{99m}Tc-labeled negatively charged polymers. *J Nucl Med.* 2006; 47:868–876.
71. Kolodgie FD, Petrov A, Virmani R, et al. Targeting of apoptotic macrophages and experimental atheroma with radiolabeled annexin V: a technique with potential for noninvasive imaging of vulnerable plaque. *Circulation.* 2003;108:3134–3139.
72. Schafers M, Riemann B, Kopka K, et al. Scintigraphic imaging of matrix metalloproteinase activity in the arterial wall in vivo. *Circulation.* 2004;109: 2554–2559.
73. Cheng Z, Mahmood A, Li H, Davison A, Jones AG. [^{99m}TcOAADT]-$(CH_2)_2$-NEt_2: a potential small-molecule single-photon emission computed tomography probe for imaging metastatic melanoma. *Cancer Res.* 2005;65:4979–4986.
74. Haubner RH, Wester HJ, Weber WA, Schwaiger M. Radiotracer-based strategies to image angiogenesis. *Q J Nucl Med.* 2003;47:189–199.
75. Jia B, Shi J, Yang Z, et al. ^{99m}Tc-labeled cyclic RGDfK dimer: initial evaluation for SPECT imaging of glioma integrin alphavbeta3 expression. *Bioconjug Chem.* 2006;17:1069–1076.
76. Liu S. Radiolabeled multimeric cyclic RGD peptides as integrin $\alpha_v\beta_3$ targeted radiotracers for tumor imaging. *Mol Pharm.* 2006;3:472–487.
77. Oltenfreiter R, Staelens L, Labied S, et al. Tryptophane-based biphenylsulfonamide matrix metalloproteinase inhibitors as tumor imaging agents. *Cancer Biother Radiopharm.* 2005;20:639–647.
78. Orlova A, Nilsson FY, Wikman M, et al. Comparative in vivo evaluation of technetium and iodine labels on an anti-HER2 affibody for single-photon imaging of HER2 expression in tumors. *J Nucl Med.* 2006;47:512–519.
79. Foss CA, Mease RC, Fan H, et al. Radiolabeled small-molecule ligands for prostate-specific membrane antigen: in vivo imaging in experimental models of prostate cancer. *Clin Cancer Res.* 2005;11:4022–4028.
80. Liu Z, Stevenson GD, Barrett HH, et al. Imaging recognition of multidrug resistance in human breast tumors using ^{99m}Tc-labeled monocationic agents and a high-resolution stationary SPECT system. *Nucl Med Biol.* 2004;31: 53–65.
81. Sharma V. Radiopharmaceuticals for assessment of multidrug resistance P-glycoprotein-mediated drug transport activity. *Bioconjug Chem.* 2004;15: 1464–1474.
82. Liu Z, Stevenson GD, Barrett HH, et al. ^{99m}Tc glucarate high-resolution imaging of drug sensitive and drug resistant human breast cancer xenografts in SCID mice. *Nucl Med Commun.* 2004;25:711–720.
83. Chapman JD, Bradley JD, Eary JF, et al. Molecular (functional) imaging for radiotherapy applications: an RTOG symposium. *Int J Radiat Oncol Biol Phys.* 2003;55:294–301.
84. Deng WP, Wu CC, Lee CC, et al. Serial in vivo imaging of the lung metastases model and gene therapy using HSV1-tk and ganciclovir. *J Nucl Med.* 2006;47: 877–884.
85. Wang HE, Yu HM, Liu RS, et al. Molecular imaging with ^{123}I-FIAU, ^{18}F-FUdR, ^{18}F-FET, and ^{18}F-FDG for monitoring herpes simplex virus type 1 thymidine kinase and ganciclovir prodrug activation gene therapy of cancer. *J Nucl Med.* 2006;47:1161–1171.
86. Yang D, Han L, Kundra V. Exogenous gene expression in tumors: noninvasive quantification with functional and anatomic imaging in a mouse model. *Radiology.* 2005;235:950–958.
87. Carlson SK, Classic KL, Hadac EM, et al. In vivo quantitation of intratumoral radioisotope uptake using micro-single photon emission computed tomography/computed tomography. *Mol Imaging Biol.* 2006;8:324–332.

88. Haberkorn U, Altmann A, Mier W, Eisenhut M. Impact of functional genomics and proteomics on radionuclide imaging. *Semin Nucl Med.* 2004;34:4–22.
89. Muller C, Bruhlmeier M, Schubiger PA, Schibli R. Effects of antifolate drugs on the cellular uptake of radiofolates in vitro and in vivo. *J Nucl Med.* 2006;47:2057–2064.
90. Muller C, Hohn A, Schubiger PA, Schibli R. Preclinical evaluation of novel organometallic ^{99m}Tc-folate and ^{99m}Tc-pteroate radiotracers for folate receptor-positive tumour targeting. *Eur J Nucl Med Mol Imaging.* 2006;33:1007–1016.
91. Baranowska-Kortylewicz J, Abe M, Pietras K, et al. Effect of platelet-derived growth factor receptor-beta inhibition with STI571 on radioimmunotherapy. *Cancer Res.* 2005;65:7824–7831.
92. Weisenberger AG, Baba JS, Kross B, et al. Dual low profile detector heads for a restraint free small animal SPECT imaging system. In: Seibert JA, ed. *Conference Record of the 2004 IEEE Nuclear Science Symposium and Medical Imaging Conference,* vol. 4. Rome, Italy: Institute of Electrical and Electronics Engineers; 2004:2456–2460.
93. Loudos GK, Nikita KS, Giokaris ND, et al. A 3D high-resolution gamma camera for radiopharmaceutical studies with small animals. *Appl Radiat Isot.* 2003;58:501–508.
94. MacDonald LR, Patt BE, Iwanczyk JD, et al. Pinhole SPECT of mice using the LumaGEM gamma camera. *IEEE Trans Nucl Sci.* 2001;48:830–836.
95. Schramm N, Wirrwar A, Sonnenberg F, Halling H. Compact high resolution detector for small animal SPECT. *IEEE Trans Nucl Sci.* 2000;47:1163–1167.
96. Kim H, Furenlid LR, Crawford MJ, et al. SemiSPECT: a small-animal single-photon emission computed tomography (SPECT) imager based on eight cadmium zinc telluride (CZT) detector arrays. *Med Phys.* 2006;33:465–474.
97. Heanue JA. Detectors and electronics design considerations for an emission-transmission medical imaging system. Electrical Engineering and Computer Sciences Department, University of California, Berkeley, Technical Report No. UCB/ERL M96/39, 1996. Available at: http://www.eecs.berkeley.edu/Pubs/TechRpts/1996/3041.htm. Accessed August 27, 2008.
98. Takahashi T, Watanabe S. Recent progress in CdTe and CdTnTe detectors. *IEEE Trans Nucl Sci.* 2001;48:950–959.
99. Kumita S, Tanaka K, Cho K, et al. Assessment of left ventricular function using solid-state gamma camera equipped with a highly-sensitive collimator. *Ann Nucl Med.* 2003;17:517–520.
100. Catana C, Wu Y, Judenhofer MS, Qi J, Pichler BJ, Cherry SR. Simultaneous acquisition of multislice PET and MR images: initial results with a MR-compatible PET scanner. *J Nucl Med.* 2006;47:1968–1976.
101. Pichler BJ, Judenhofer MS, Catana C, et al. Performance test of an LSO-APD detector in a 7-T MRI scanner for simultaneous PET/MRI. *J Nucl Med.* 2006;47:639–647.
102. Funk T, Despres P, Barber WC, Shah KS, Hasegawa BH. A multipinhole small animal SPECT system with submillimeter spatial resolution. *Med Phys.* 2006;33:1259–1268.
103. Funk T, Sun M, Hasegawa BH. Radiation dose estimate in small animal SPECT and PET. *Med Phys.* 2004;31:2680–2686.
104. Loevinger R. *MIRD Primer for Absorbed Dose Calculations.* New York, NY: Society of Nuclear Medicine; 1991.
105. Amundson SA, Bittner M, Meltzer P, Trent J, Fornace AJ Jr. Induction of gene expression as a monitor of exposure to ionizing radiation. *Radiat Res.* 2001;156:657–661.
106. Patchen ML, MacVittie TJ, Souza LM. Postirradiation treatment with granulocyte colony-stimulating factor and preirradiation WR-2721 administration synergize to enhance hemopoietic reconstitution and increase survival. *Int J Radiat Oncol Biol Phys.* 1992;22:773–779.
107. Samarth RM, Kumar A. Radioprotection of Swiss albino mice by plant extract *Mentha piperita* (Linn.). *J Radiat Res (Tokyo).* 2003;44:101–109.
108. Stevenson GD. The animal in animal imaging. In: Kupinski MA, Barrett HH, eds. *Small-Animal SPECT Imaging.* New York, NY: Spinger Science+Business Media, Inc.; 2005:87–100.
109. Meikle SR, Kench P, Weisenberger AG, et al. A prototype coded aperture detector for small animal SPECT. *IEEE Trans Nucl Sci.* 2002;49:2167–2171.
110. Goertzen AL, Jones DW, Seidel J, Green MV. First results from the high-resolution mouseSPECT annular scintillation camera. *IEEE Trans Med Imaging.* 2005;24:863–867.
111. Bequé D, Nuyts J, Bormans G, Suetens P, Dupont P. Characterization of pinhole SPECT acquisition geometry. *IEEE Trans Med Imaging.* 2003;22:599–612.
112. Metzler SD, Greer KL, Jaszczak RJ. Determination of mechanical and electronic shifts for pinhole SPECT using a single point source. *IEEE Trans Med Imaging.* 2005;24:361–370.
113. Wang Y, Tsui BMW. Pinhole SPECT with different data acquisition geometries: usefulness of unified projection operators in homogeneous coordinates. *IEEE Trans Med Imaging.* 2007;26:298–308.
114. Andreyev A, Defrise M, Vanhove C. Pinhole SPECT reconstruction using blobs and resolution recovery. *IEEE Trans Nucl Sci.* 2006;53:2719–2728.
115. Chen YC, Furenlid LR, Wilson DW, Barrett HH. Calibration of scintillation cameras and pinhole SPECT imaging system. In: Kupinski MA, Barrett HH, eds. *Small-Animal SPECT Systems.* New York, NY: Springer Science+Business Media Inc.; 2005:195–201.
116. Rehfeld N, Alber M. A parallelizable compression scheme for Monte Carlo scatter system matrices in PET image reconstruction. *Phys Med Biol.* 2007;52:3421–3437.
117. Lindsey ML, Escobar GP, Dobrucki LW, et al. Matrix metalloproteinase-9 gene deletion facilitates angiogenesis after myocardial infarction. *Am J Physiol Heart Circ Physiol.* 2006;290:H232–H239.
118. Cherry SR, Sorenson J, Phelps ME. *Physics in Nuclear Medicine.* Philadelphia, PA: Saunders; 2003.
119. Metzler SD, Bowsher JE, Greer KL, Jaszczak RJ. Analytic determination of the pinhole collimator's point-spread function and RMS resolution with penetration. *IEEE Trans Med Imaging.* 2002;21:878–887.
120. Metzler SD, Bowsher JE, Smith MF, Jaszczak RJ. Analytic determination of pinhole collimator sensitivity with penetration. *IEEE Trans Med Imaging.* 2001;20:730–741.
121. Zhou R, Thomas DH, Qiao H, et al. In vivo detection of stem cells grafted in infarcted rat myocardium. *J Nucl Med.* 2005;46:816–822.